Rethinking the Polar Cap: ULF asymmetry at the highest corrected geomagnetic latitudes

Kevin D. Urban,[1] Andrew J. Gerrard,[1] Louis J. Lanzerotti,[1] and Allan T. Weatherwax[2]

Abstract. Using a unique high-latitude network configuration of ground-based magnetometers in Antarctica, the day-to-day, longer-term, and statistical features of broadband Pc5-6/Pi3 ultra-low frequency (ULF) hydromagnetic activity at polar cap latitudes is presented. Over a 63-day relatively quiet interval in early 2001, it is shown that there is both a day-to-day and a statistical asymmetry between two ground sites (AGO5 and AGO6) at about ∼86° corrected geomagnetic (CGM) latitude, separated 12 hours in magnetic local time (MLT). Comparing the near-CGM-pole ULF activity from the two sites with concurrent activity at cusp and sub-cusp sites in the network, it is found that hydromagnetic activity at AGO6 is strikingly similar to a cusp-latitude site. However, the observations at AGO5 stand out as truly unique. The results suggest that ULF studies at high CGM latitudes cannot freely be used to infer the ULF activity at other sites of similar CGM latitude, but separated in MLT. This generalizes to meridional chains and other types of localized, but scattered networks of ground-based instrumentation at high CGM latitudes: statistical maps in CGMLat/MLT coordinates constructed from such restricted networks are not necessarily directly applicable to any other ground sites than those used to construct the map. Given our observations, the utility of CGM coordinates in the polar cap is questioned which has implications for conjugacy/mapping studies at polar latitudes in general. We show that the AGO5 location is a better representation of a central point in the polar cap than the CGM pole.

1. Introduction

Ground-based magnetometers situated at the highest geomagnetic latitudes are in the position to study hydromagnetic features of the outermost boundaries of the magnetosphere and of open field lines (those geomagnetic field lines merged with the interplanetary magnetic field (IMF)). However, despite the frequent presence of broad- and narrowband ultra-low frequency (ULF) hydromagnetic power at cusp latitudes (e.g., *Ballatore et al.* [1998]) and deeper into the polar cap (e.g., *Yagova et al.* [2002, 2004]), the structure and dynamics of the hydromagnetic polar cap and how these features relate to ionospheric and magnetospheric regions observed by spacecraft is not well understood (e.g., see the reviews by *Pilipenko and Engebretson* [2002] and *Engebretson et al.* [2006]).

Early ground-based studies at cusp latitudes aimed to characterize the hydromagnetic ULF activity and utilize this characterization in describing global features of the magnetosphere (e.g., as reviewed and referenced in *Troitskaya et al.* [1980], *Troitskaya* [1985], and *Troitskaya and Bolshakova* [1988]). These early studies found that changes in cusp structure and dynamics are associated with changes in long-period irregular pulsations (3-10 minute periodicities) in the polar cap, which the authors called irregular pulsations at cusp latitude (IPCL)—now more commonly known as broadband Pc5-6/Pi3 pulsations. Using this association, *Bolshakova et al.* [1975] and *Troitskaya and Bolshakova* [1977] looked at ways to utilize the cusp-latitude broadband Pc5-6/Pi3 pulsations to monitor the dayside cusp. *Bolshakova et al.* [1975] claimed to be able to identify the polar boundary of the cusp with signatures in their ground-based ULF data.

Wolfe et al. [1996] and *Papitashvili et al.* [1996] both reported on high-latitude hydromagnetic ULF wave observations that were quoted as new discoveries, indicating that such ground-based studies of the hydromagnetic polar cap were more-or-less still considered in their infancy 20 years later. Using magnetometers situated between 77.2°S-83.3°S corrected geomagnetic (CGM) latitude (CGMLat), *Papitashvili et al.* [1996] reported on low-magnitude (3-5 nT), long-period (15-17 minute) magnetic pulsations deep in the southern polar cap, which appeared to be exclusive to northward IMF conditions during austral winter, but which additional high-latitude magnetometer data from the northern hemisphere showed to occur during the equinoxes as well. They noted that similar Pc6-band pulsations did not appear in the variations of the IMF. It is likely they were observing Pc5-6 resonances on extended closed field lines (*Mathie and Mann* [2000], *Urban et al.* [2011]). Alternatively, *Wolfe et al.* [1996] argued that the hydromagnetic ULF waves they observed—large-amplitude (10-20 nT) Pc5 waves—occurred on open field lines. On a moderately quiet day (Mean(Kp) ≈ 3.67) in austral winter, *Wolfe et al.* [1996] took advantage of the wide (∼ 75°) separation in CGM longitude (CGM-Lon) at 80°S CGMLat provided by the recently-deployed Automated Geophysics Observatories (AGOs) AGO1 and AGO4 in conjunction with the magnetometer at McMurdo Station (MCM), to synoptically investigate the high-latitude azimuthal structure of hydromagnetic activity. The authors show three instances of Pc5 waves observed concurrently at all sites. Using particle precipitation data from a nearby polar-orbiting spacecraft during these three different intervals (two when the magnetometers were in the dusk/pre-midnight sector, one when they were in the dawn sector),

[1]Center for Solar-Terrestrial Research, New Jersey Institute of Technology, Newark, New Jersey, USA.
[2]School of Science and Engineering, Merrimack College, North Andover, Massachusetts, USA.

0148-0227/16/$9.00

the authors argue that all three sites were likely on open field lines.

Instead of relying on the availability of nearby spacecraft observations or the verity of mapping techniques, it is desirable to be able to use data from ground-based magnetometers themselves as a means of delineating between open and closed geomagnetic field lines, as *Bolshakova et al.* [1975] attempted to do. However, this has been a nontrivial pursuit. Later studies have shown that though broadband Pc5-6/Pi3 ULF activity at high latitudes is often associated with the cusp, it is unlikely that there exist broadband Pc5-6/Pi3 signatures unique to the cusp/cap boundary or the open/closed field line boundary [OCB] in general (e.g., *Engebretson et al.* [1995], *Pilipenko and Engebretson* [2002], *Engebretson et al.* [2006], *Pilipenko et al.* [2015]). For example, *Pilipenko et al.* [2015] compared the broadband Pc5-6/Pi3 maxima along the Svalbard/IMAGE meridian chain of magnetometers (ranging between 67.2°N-80.9°N CGMLat) to cusp location identifications derived from three independent methods (overhead SuperDARN radar beam data, model prediction *Newell et al.* [2006], and DMSP boundary identifications), showing that the IPCL maxima occur $1-5^{\circ}$ equatorward of the cusp. Other studies have demonstrated that instead of irregular, broadband Pc5-6/Pi3 pulsations, narrowband Pc5-6 pulsations could possibly indicate this dayside OCB (e.g., *McHarg et al.* [1995], *Ables et al.* [1998], *Lanzerotti et al.* [1999]), and possibly on the nightside as well (*Urban et al.* [2011]).

Since features identified at the highest geomagnetic latitudes likely can speak to the nature of hydromagnetic activity on open field lines, if progress is to be made on using high-latitude ground-based magnetometer data to delineate between open and closed field lines, it is imperative that very high-latitude data itself be thoroughly investigated as a function of CGMLat and magnetic local time (MLT) (e.g., *Yagova et al.* [2002]), and correlated and compared with colocated instrumentation (e.g., *Weatherwax et al.* [1997]). If one can show that unique hydromagnetic signatures exist in the polar cap, it remains possible that such ground-based magnetometer data sets could be used for open/closed field line and/or boundary determination. In this regard, ULF signatures unique to the polar cap have been identified by *Yagova et al.* [2002], who used a CGM-meridional chain of four magnetometers in Antarctica ranging between ∼69°S-87°S CGMLat in effort to characterize and compare auroral, cusp, and cap latitude broadband Pc5-6/Pi3 (specifically, periodicities between 3.33-16.67 minutes). Both statistically and in selected case studies, *Yagova et al.* [2002] depicted how various spectral features change along this magnetic meridian during nighttime hours, showing that [1] there exists a minimum in Pc5-6/Pi3 ULF power near ∼80°S CGMLat in their data, [2] that auroral latitudes generally housed more higher-frequency ULF content than found in the nominal polar cap, [3] that the broadband polar cap oscillations were coherent among the three cap sites along the magnetic meridian, and [4] that such oscillations were decoupled from similar phenomena at auroral latitudes. Importantly, item [4] tells us that the polar cap supports ULF waves that are independently sourced, not simply residual activity from auroral latitudes; previous to *Yagova et al.* [2002], the polar cap was often considered to be hydromagnetically quiet, any observed ULF power being residual of auroral region ULF waves (e.g., see review by *Engebretson et al.* [2006]). To ensure that these ULF waves observed in *Yagova et al.* [2002] were unique to the polar cap, *Yagova et al.* [2004] looked at data from a scattered network of 16 ground-based magnetometers in Antarctica to study the synoptic distribution of broadband Pc5-5/Pi3 power in the summertime polar cap. They were able to further verify that the hydromagnetic polar cap is not merely a residual phenomenon from lower-latitude hydromagnetic activity.

The high-latitude region in both the northern and southern hemispheres is difficult to populate with magnetometers, so we often rely on studies like *Yagova et al.* [2002] which use several magnetometers to characterize the entire polar cap. In this vein, many studies have allowed a single magnetometer at a given high-latitude CGMLat to characterize all other points along the given CGMLat parallel, in that such studies statistically characterize that CGMLat as a function of magnetic local time [MLT] as if it is representative on all other points of the parallel. Expanding upon this, chains of magnetometers along a given CGM meridian have been used construct CGMLat/MLT maps of ULF activity with the assumption that these maps are directly applicable to sites located away from the chain. The assumption is that such generalizations can fruitfully be made using CGM coordinates.

However, these assumptions might not hold, as indicated in the plots found in *Ballatore et al.* [1998], where the authors use an azimuthal array of four ground-based magnetometers at 80°S CGMLat to statistically characterize high-latitude Pc5 power at this CGMLat. The Pc5 power at each of the four sites exhibited a seasonal dependence by which the Pc5 power was found to be higher during local summer than during the local winter, a feature they ascribed to the increased ionospheric conductance during the sunlit summer season. They further showed that the dayside summertime enhancement was more significant than that found on the nightside, attributing this to the seasonally-dependent location of the magnetospheric cusp. However, as noted by *Yagova et al.* [2004], *Ballatore et al.* [1998] did not elaborate much on the observation that the statistics at each site did not conform to each other very well.

Much deeper into the nominal CGM polar cap, *Detrick and Lanzerotti* [2001] also observed differences in their statistical characterization of geomagnetic activity at two high-latitude Antarctic sites (AGO5 and AGO6) residing on nearly the same CGMLat (∼86°S), but separated in MLT by 12 hours. The authors looked at the time series data from AGO5 and AGO6 to study geomagnetic quiet-time (Sq) variations at very high geomagnetic latitudes. Analysis of the data from both sites suggested that Sq variations near the CGM pole is a factor of two or more than quoted by concurrent Sq models, independent of season. *Detrick and Lanzerotti* [2001] interpreted the observed azimuthal asymmetry at AGO5 and AGO6 as indicative of large differences in the deep mantle conductivity under the ice at AGO5 and AGO6. Independent of the cause, this asymmetry in the two data sets highlights that diurnal/Sq statistics derived from one site at a given CGMLat are not representative another site at the same CGMLat. Furthermore, by comparing one-month averages of spectral and cross-spectral features at AGO5 and AGO6, *Yagova et al.* [2004] highlighted a discrepancy in the Pc5-6/Pi3 band: the average power at AGO6 takes on a MLT dependence characteristic of sites at ∼80°S CGMLat rather than match the statistics at AGO5. They interpret these differences as due to the importance of geographic, in addition to geomagnetic, coordinates in organizing hydromagnetic phenomena at polar cap latitudes.

In this paper, we look more deeply at the differences inherent at these two cross-polar, near-CGM-pole sites. We show that AGO6 is hydromagnetically akin to the cusp-latitude site MCM and very different from the activity found at AGO5. We argue that the differences observed at AGO5 and AGO6—in addition to some of the ascriptions provided by *Detrick and Lanzerotti* [2001] and *Yagova et al.* [2004]—arise in part due to a misrepresentation of sites in the nominal polar cap region given by CGM coordinates. The ULF symmetry in AGO6 and MCM and the asymmetry found between AGO6 and AGO5 cannot be explained by their

CGM coordinates. However, the seemingly inexplicable features clear up quite a bit if one discards CGM coordinates in favor of another system for organizing polar cap hydromagnetic phenomena. Specifically, by simply considering the central point of the polar cap to be at or very near the location of AGO5, and defining magnetic latitude parallels as equidistant angular displacements from AGO5, both the uniqueness of AGO5 data and the striking similarity between AGO6 and MCM clear up. Interestingly, if instead of the AGO5 location, one uses the nearby location defined by the axial polar point of the eccentric dipole [ED] model, one also can physically motivate why a change-of-coordinates such as this better organizes the polar cap ULF activity.

Lastly, independent of the cause of observed azimuthal asymmetries in ULF power at high latitudes, we emphasize that the differences at AGO5 and AGO6 outlined here (and in *Ballatore et al.* [1998], *Detrick and Lanzerotti* [2001], and *Yagova et al.* [2004]) inherently disallow one to use a small, localized network of magnetometers to construct CGMLat/MLT statistical ULF activity maps which can then be used to infer the ULF activity located in any other region of similar CGMLats, but largely displaced in CGMLon. Instead, if one is using CGM coordinates, real-time synoptic coverage must be used to characterize the hydromagnetic polar cap. In light of this, the location of AGO6 is extremely important since the magnetometer distribution in this longitudinal region of CGM coordinates is extremely sparse.

2. Experimental Setup

The U.S. network of ground-based geospace observatories in Antarctica covers a geomagnetic azimuthal range of ∼187°, and includes six AGOs (AGO1-AGO6), and two additional instrument suites at the manned sites South Pole [SPA] and MCM. (See reviews by *Doolittle and Mende* [1985], *Dudeney et al.* [1998], *Mende et al.* [2009], and *Melville et al.* [2014] for more information on the U.S. AGOs.)

In CGM coordinates, the network consists of three quasi-meridional arrays with AGO5 as their common point: [i] AGO5-AGO1-SPA-AGO2 (∼19° E CGMLon), [ii] AGO5-AGO4-AGO3 (∼41° E CGMLon), and [iii] AGO5-MCM (∼327° E CGMLon). The network also supports two closely-spaced quasi-longitudinal arrays: [i] AGO2-AGO3 (∼70° S CGMLat) and [ii] AGO1-AGO4-MCM (∼80° S CGMLat). Lastly—and most importantly for this paper—the network supports a near-polar pair of observatories, separated in magnetic local time by 12 hours: AGO5 at ∼87°S CGMLat and AGO6 at ∼85°. The AGO5 and AGO6 locations were specially selected to conduct cross-polar comparisons with the impression that the CGM pole best represented a central point within the polar cap, as opposed to the polar points associated with centered dipole [CD] and the eccentric dipole [ED] models (see *Fraser-Smith* [1987] for more on ED and CD coordinates). AGO6 last recorded data in 2001, reducing the current network coverage to a ∼75° sector (just smaller than a MLT quadrant at any given time). The AGO5-AGO6 pair is the only of its kind at such high geomagnetic latitudes and offers the possibility of investigating the evolution of cross-polar, near-pole ULF power simultaneously. Data recorded at AGO6 is additionally important due to the sparsity of instrument suites in its vicinity of CGMLon.

During the interval of this study (days 27-89 of 2001), four of the magnetometers in the U.S. Antarctic network (AGO5, AGO6, MCM, and SPA) recorded uninterrupted vectorial data (see Figure 1). Table 1 gives the geographic and corrected geomagnetic locations of the four sites from this network used in this study. Given the recent criticism of numerical approximations of CGM coordinates at polar latitudes by *Shepherd* [2014], we provide CGM coordinates using both the commonly-used algorithm provided by Johns Hopkins University / Applied Physics Laboratory [JHU/APL] (code written by R. Barnes) and Shepherd's field-line traced coordinates. (For more on CGM coordinates and their approximations, see *Gustafsson* [1984]; *Baker and Wing* [1989]; *Gustafsson et al.* [1992]; *Papitashvili et al.* [1992]; *Heres and Bonito* [2007]; *Shepherd* [2014].)

3. Data Analysis and Observations

The fluxgate magnetometers used in this study measure the relative variation of the geomagnetic field at a 1-second cadence. To reduce noise, discard extreme outliers (spikes), and account for missing or bad point measurements, the data streams at all stations are downsampled to a 10-second temporal resolution, resulting in a Nyquist period of 20 seconds.

As seen in the top panel of Figure 1, all sites exhibit a diurnal variation with a peak-to-trough amplitude that appear to vary with geomagnetic activity, which is relatively quiet-to-moderate for most of the interval. Of the 51 days prior to DOY 78, the maximum daily Kp (Figure 1, top panel) breaches 4.0 on only 8 days (∼15.7%), whereas this occurs on 8 of 12 days between 78-89 (∼75%). Over the entire 63-day interval, the maximum daily Kp breaches 5.0 on only 7 days (29, 64, 78, 79, 82, 86, and 87). The median daily Kp reaches or rises above 5.0 on DOYs 79 and 87 only (days in which we see the largest depressions in Dst during the interval). The median (mean) Kp index over the entire interval is 1.67 (1.89). The Dst index (Figure 1, panel 2) illustrates the 63-day interval as ranging over a diverse set of quiet-to-moderate geomagnetic conditions, which is useful in understanding polar cap hydromagnetic dynamics in the absence of extreme events.

3.1. Dynamic Power Spectra

3.1.1. Method

Before spectral analysis, each 63-day data stream (N_{Tot} = 544320 data points (DP), Δt = 10) is mean-subtracted and digitally high-pass filtered to remove trends and periodicities with timescales longer than four hours. In light of some of the longer Pc6-band periodicities observed to occur in the polar cap (e.g., 30-45 minute periodicities), and the fact that a window length in the time domain should be roughly 3-4 times the longest period one hopes to resolve, we chose to subset the filtered data streams into 4-hour segments, stepped forward in time every hour (N=1440 DP, N_{step}=360 DP). This results in N_{seg} data segments for each component at each site, where $N_{seg} = floor(\frac{N_{tot}-N}{N_{step}} + 1) =$ 1509.

To estimate the power spectra for each N-point data segment, we start by computing the short-time discrete Fourier spectra using the "over-normalized" forward FFT (periodogram) implemented in IDL:

$$X^w[m,j] = \frac{1}{N}\sum_{k=0}^{N-1} w[k]x[m+k-N/2]e^{-2\pi ijk/N} \quad (1)$$

where m refers to the mth data segment centered at $m\Delta t$, j refers to the jth Fourier frequency, $f_j = j\Delta f$, and $\Delta f = j/(N\Delta t)$ denotes the DFT frequency spacing. The superscript w emphasizes that the DFT spectra of the data segments x[m+k-N/2] are dependent on the chosen window function, $w[k]$. It is not possible to forgo the application of a data window since the default DFT/FFT spectra are rectangle-windowed—that is, $w_R[k] = 1$ over the interval

of analysis, $[t_0, t_N] = [0, N\Delta t]$, and zero elsewhere. In practice, for colored noise spectra, rectangularly-windowed power spectra result in spectral indices that are biased low because of high-frequency power estimates that are biased high—the result of a digital phenomenon known as spectral leakage (e.g., *Harris* [1978], *Heinzel et al.* [2002]). A carefully-chosen window can reduce this undesirable effect, and others such as scalloping loss, resulting in spectra that might be considered more physically-meaningful than spectra computed without this consideration.

To reduce spectral leakage and scalloping loss in our analysis, we mean-subtract and apply the Hanning taper to each time-domain segment prior to computing each FFT, resulting in N_{seg} modified periodograms for each given data stream:

$$P_X^w[m,j] = c|X^w[m,j]|^2 \tag{2}$$

where c is a constant dependent on the type of forward FFT that is used, the choice of window, whether one is computing power spectral densities (PSDs) or power spectra (PS), and whether the spectrum is one- or two-sided. To ensure the spectral amplitudes are physical and not dependent on the length of the data window, we compute the PS instead of the PSD of each data segment; the two are related by equivalent noise bandwidth (ENBW), $\delta f = s\Delta f$, of the chosen window ($PS^w[m,j] = PSD^w[m,j]\delta f$), where s is a "smear factor" indicating that there is a slight frequency resolution trade-off with the reduction of spectral leakage.

All things considered, our modified periodograms ultimately take on the form:

$$P_X^w[m,j] = 2N^2 \left(\frac{|X^w[m,j]|}{\sum_{k=0}^{N-1} w[k]} \right)^2, \qquad j \in [1, N/2] \tag{3}$$

where the halved frequency index denotes that we are considering the "one-sided" modified periodogram, and the factor of 2 is necessary to account for the total root-mean-square (RMS) power available to each frequency band in this representation. (To convert to peak amplitudes, multiply by two and take the square root.)

Finally, to reduce noise in all spectral estimates, the power estimates at each time step in the dynamic spectra (illustrated in Figure 2 and Figure 3) were geometrically averaged (log-smoothed) with their nearest neighbors in time and in frequency.

$$\widehat{P}_X^w[m,j] = \left(\prod_{k=j-1}^{j+1} \left(\prod_{l=m-1}^{m+1} P_X^w[l,k] \right)^{1/3} \right)^{1/3} \tag{4}$$

Geometric smoothing in frequency reduces the bias towards higher power from the lower frequency neighbor. Given that the geomagnetic power at each Fourier frequency also follows a distribution akin to a log-normal or power-law distribution, the geometric mean is again desirable when smoothing in time to reduce biasing estimates towards higher neighboring values.

3.1.2. Observations

In Figure 2 and Figure 3, we plot the horizontal and vertical power spectra, respectively, in the log-log domain over the 63-day interval. The horizontal power spectra are defined as the sum of the magnetic north and magnetic east power spectra, $\widehat{P}_H^w = \widehat{P}_N^w + \widehat{P}_E^w$, where we denote the horizontal, magnetic north, and magnetic east components with the subscripts H, N, and E, respectively. The overplotted black traces in Figure 2 and Figure 3 represent the integrated ULF power.

The chosen window length of four hours was to avoid prematurely ruling out the significance (or lackthereof) of frequencies lower than the nominal Pc6 band, which we refer to as the radically-low frequency (RLF) band (1-4 hours). Note that frequency power in the RLF band has the potential to be contaminated by spatial structure in which local time differences in background power could be confused as temporal evolution, and so should be interpreted with caution. In much of the analysis below, however, the RLF band seems to naturally extend the Pc6 band during the appropriate times at the high-latitude sites.

Due to the large dynamic range (spanning 9-10 orders of magnitude) of the geomagnetic spectra, the power spectra shown in Figure 2 and Figure 3 are capable of little more than illustrating the well-known fact that lower-frequency ULF bands carry more power than their higher-frequency counterparts. In terms of how the power at each frequency varies from day to day and over longer time scales, one might argue that the overplotted integrated ULF power traces tell us just as much as the full contour.

However, what is immediately noticeable in both the contour representation and the integrated power is the presence or absence of a strong diurnal variation—a feature which serves to highlight AGO5 as a unique high-latitude site. While both MCM (∼80°CGMLat) and AGO6 (∼85°S CGMLat) have emphatically strong diurnal power variations, such a variation at AGO5 is weak to nearly non-existent at times. The local geomagnetic activity at SPA (∼74°CGMLat) is strongly driven by numerous sources (e.g., auroral electrojets from nominally-lower latitudes, cusp emission from nominally-poleward latitudes, and strong substorm driving); this serves to make it appear as if SPA similarly does not have a strong diurnal variation, though it does (as is shown later).

The similarity between AGO6 and MCM and the dissimilarity between AGO6 and AGO5 in this regard indicates that the hydromagnetic activity at AGO6 (at least during this interval) has the appearance of that found at a cusp-latitude site. In other words, if one disregards the CGM coordinates of the Antarctic sites and told only the story as outlined by the data analysis, one would not consider AGO6 as deep in the polar cap as the CGM coordinates suggest, but to be in the same general polar cap region as MCM. Without regard to CGM coordinates, the basic PSD data tells us that the region housing AGO5 is unique and likely deserving of a classification of its own.

3.2. Median-Relative Dynamic Spectra

3.2.1. Method

For colored-noise spectra like the computed geomagnetic power spectra, the details are more transparent if some transformation is applied that in one way or another "whitens" the spectra (i.e., strips the spectra of the large dynamic range in some way, while retaining as much spectral information as possible). In this paper, to better address the large dynamic range in the power spectra, we have computed the median-relative (MR) spectra by dividing the power at each frequency by the median power at that frequency over the 63-day interval. At each site, the MR spectra effectively put the relative growth and decay in power at each Fourier frequency on the same scale, indicating how significant (or insignificant) the power at a given frequency is relative to its median value over a given time interval, τ.

To construct MR spectra, first the median power spectrum is computed at each site (Figure 4) by simply taking the median power value at each Fourier frequency in the unsmoothed power spectra (Equation 3) over the full 63-day interval:

$$\widetilde{P}_X^{w,\tau}[j] = MED_m(P_X^w[m,j],\tau) \quad (5)$$

where the subscript τ denotes that the median is computed over a given interval and is subject to change given a different interval of time; however, for each frequency bin, there are 1509 power estimates ranging over quiet-to-moderate geomagnetic activity, which gives confidence that it is a suitable estimate of background power at these sites. The MR dynamic spectra (Figure 5 and Figure 6) are then computed by dividing the power spectra (Equation 3) at each time step by the site's median spectrum (Equation 5):

$$MR_X^{w,\tau}[m,j] = \frac{P_X^w[m,j]}{\widetilde{P}_X^{w,\tau}[j]} \quad (6)$$

The division of the dynamic spectra by the median spectrum transforms each spectral estimate at a given time step and Fourier frequency into a scale factor where values in the range [0,1) represent power less than the median at that frequency, values in the range (1,∞) represent power greater than the median, and where a value of 1.0 indicates the median power. Figure 5 and Figure 6 are plotted in the log domain, in which depletions (enhancements) are represented by numbers less (greater) than zero. Visually this translates to the following: blues denote significantly less power than the median at the given frequency, while reds denote significantly more power than is median; yellow denotes the median power at a given frequency. One can clearly pick out both diurnal variation and longer-term evolution in the ULF power spectra.

The median spectrum (rather than an average spectrum) was chosen as the proper background to measure relative power values because the power at each frequency approximates a log-normal or power-law distribution better than a normal distribution. In such a case, the average does not measure central tendency, for which it is biased too high. Given a log-normal distribution, the geometric mean does measure central tendency. Although the median spectral values very closely approximated the geometric mean spectral values (not shown), the median background was selected given its nonparametric and robust nature against deviations in a statistical distribution as a measure of central tendency.

Finally, in Figure 5 and Figure 6, to reduce noise in all MR spectral estimates, the individual estimates were geometrically averaged (log-domain smoothed) with their nearest neighbors in time and frequency.

$$\widehat{MR}_X^{w,\tau}[m,j] = \left(\prod_{j=k-1}^{k+1} \left(\prod_{m=l-1}^{l+1} MR_X^{w,\tau}[m,j] \right)^{1/3} \right)^{1/3} \quad (7)$$

For the median-relative spectra, the log-domain smoothing is essential since these estimates are scale factors which are not summable quantities (by definition, a simple average sums and divides by N). In other words, considering that the MR spectra are scale factors, the range [0,1) represents a median-relative depletion in power and the range (1,∞) represents a median-relative enhancement. Given such a small subset representing depletions, averaging neighboring scale factors will be biased high, falsely giving the impression of enhancements. This bias is removed when smoothing scale factor in the log domain, where the depletions take on the range (-∞,0) and the enhancements take on (0,∞), effectively putting enhancements and depletions on an equal footing in regards to smoothing.

We again look at horizontal and vertical data, where the individual horizontal MR spectra are found by plugging the unsmoothed horizontal dynamic spectra, $P_H^w = P_N^w + P_E^w$, into Equations 5-6, and smoothed in Equation 7.

3.2.2. Observations

The horizontal median spectrum from each of the four sites is shown in Figure 4. The cusp-latitude site (MCM) and the two deep polar cap sites (AGO5 and AGO6) have essentially the same background spectrum. The MR spectra in Figure 2 and Figure 3 show the horizontal and vertical MR spectra, respectively, which describe how the power spectrum at each site evolves relative to the background spectrum at the site. Interestingly, despite sharing a very similar background spectrum, the MR spectra at the three highest-latitude sites can be seen to differ in a significant way. A strong diurnal variation is observed at all sites with the exception of AGO5, which only follows the longer-term evolution seen at the other two sites.

In the horizontal MR spectra (Figure 5), we see that the power often scales homogeneously across the Pc3-RLF band (columnar structures), depicting that oftentimes at any of these sites, power across the ULF bands grow in tandem by the same factor. This repeating columnar pattern is largely due to the local-time variation at the site as can be visually picked out by associating columns with tickmarks. This columnar, daily growth and decay of ULF power is mostly noticeable at MCM and AGO6 (although in the local-time distributions described below, it is also a feature at SPA).

In addition to such homogeneous scaling, there also exist times at each site where clear growth and decay relative the median spectrum occurs nonuniformly. For example, instances when the MR growth factor across the frequency bands is not constant, but varies fairly monotonically like that seen on DOYs 40-41 when SPA has clearly stronger Pc3 enhancements than growth in the lower-frequency bands. At other times, the nonuniformity is not monotonic, but it is still fairly continuous across the frequency bands—like that seen at AGO5 on DOYs 41-44 where the MR factor indicates growth in RLF band, decay in the Pc5-6 band, and growth again in the Pc3-4 band.

Lastly, there exist both broad- and narrowband types of distinctly discontinuous-looking phenomena. For example, on DOY 75, SPA and MCM record a concurrent strong broadband Pc5 enhancement (red) in stark contrast to the surrounding band in which depletions (blues) were recorded. On DOYs 41-44, AGO5 has an interesting discontinuous growth in the bands surrounding the Pc5-6 band, while the Pc5-6 band itself remains steadfastly median to sub-median (yellow to bluish green).

Discontinuous narrowband features look like distinct pockmarks in the horizontal spectra at various time steps; these correspond to significant narrowband peaks rising well above the colored noise background.

The features described in the horizontal MR spectra (Figure 5) often stand out more starkly in the vertical MR spectra as shown in Figure 6.

In regard to the current study, the most important feature in the MR spectra are the diurnally-repeating columnar structures frequently observed in the MCM and AGO6 MR spectra, but to a much lesser extent in the AGO MR spectra. The fact that the the median spectra at at AGO5, AGO6, and MCM (Figure 4) over the 63-day interval that are nearly identical across the Pc3-RLF frequency band makes this all the more striking. The nearly-identical median spectra in juxtaposition to the median-relative dynamic spectra tell us that the same ULF background exists at all three polar cap sites—and that whatever is strongly modulating the power diurnally at MCM and AGO6 is not doing so at AGO5 (AGO5 does have occasional diurnal variation, but it has a much weaker, smeared appearance than that found at AGO6 or MCM). In line with the conclusions of *Ballatore et al.*

[1998], it seems likely that this diurnal driving at MCM and AGO6 is due to a near-noon feature like the cusp.

3.3. Median ULF Power versus Local Time

3.3.1. Method

Plotted in Figure 7 are the local-time median power distribution for magnetic north, magnetic east, and the vertical component at the four sites under study in Pc4, Pc5, and Pc6 bands. In each local-time power plot, SPA is blue, MCM is light blue, AGO6 is light red, and AGO5 is red.

To investigate diurnal variations further, we computed the median (background) power in the Pc4, Pc5, and Pc6 bands as a function of local time for all three geomagnetic components at each site (Figure 7).

To compute such local time functions, power spectra were first computed in a similar fashion as previously described in the section on dynamic power spectra. However, to ensure independent local time estimates of power, 1-hour windows stepped forward in time every 1-hour were used instead of 4-hour windows stepped forward in time at 1-hour intervals. Furthermore, no smoothing in frequency or time was implemented. Instead, the band power was then computed in the Pc4, Pc5, and Pc6 bands for each spectrum, resulting in three 1-hour resolved time sequences over the 63-day interval. Finally, to compute the Pc4, Pc5, and Pc6 local time curves, the median band power for each of the 24 UT hours was computed from the associated 63 estimates.

The median was chosen here as a background measure due to its robust and nonparametric nature as a measure of central tendency. As previously indicated, the power in each individual Fourier frequency is approximately log-normal or power-law distributed over the 63-day interval; this implies that the summation/integration of these frequencies to compute band power also result in similarly non-normal distributions (e.g., the sum of log-normal random variables is approximately log-normal).

3.3.2. Observations

The most striking features are (1) how much less median power AGO5 has relative to the other sites, (2) that AGO6 and MCM have strikingly similar local-time median power distributions in most components in all frequency bands, (3) that AGO5 is the only site that is strongly horizontally polarized, and (4) morphologically-speaking, AGO5 is stands out as unique, especially when comparing directly to AGO6 and MCM.

Although AGO5 has much lower power overall across the various ULF bands, one can pick out possible diurnal features in Figure 7, made easier by plotting AGO5 median and mean power curves on this lower scale of power (not shown). Whereas the median power curves at MCM and AGO6 have near-noon enhancements in most of the components and ULF bands about 5-10 times the power throughout the day, the enhancements at AGO5 are not as sudden or emphatic being only about 2-3 times the lower values on the curves.

The magnetic north component across the Pc4-Pc6 bands at AGO5 has two of these gradual enhancements. The first enhancement occurs in the post-midnight/pre-dawn MLT region. Interestingly, the enhancement begins peaking closer to midnight for long periodicities (∼0100-0600 MLT in the Pc6 band, ∼0200-0600 MLT in the Pc5 band, and ∼0300-0600 in the Pc4 band). The other enhancement across the ULF bands in the magnetic north component are slighter and maximize near- or post-noon.

In the magnetic east component at AGO5, there is an apparent dual peak structure again. The first enhancement occurs at or very shortly after local midnight. There is then a 40-50% dip in power between 0300-0400 MLT in all bands, followed by another enhancement between ∼0700-0900 MLT (this is emphatic when plotting these curves on their own scale). This second enhancement is followed by a strong drop beginning at ∼1000 and diminishing to ∼25-40% of the previous peak's power at noon. The power in all bands begins to grow again immediately post-noon, building up towards the near-midnight peak.

At all local times and in all three bands, the vertical component holds about a third or less of the power that is found in the magnetic north and magnetic east components. This tells us that the hydromagnetic power at AGO5 is mostly contained in the horizontal plane. This does not strictly hold at the other sites, especially AGO6 and MCM which have significant vertical power in some of the bands.

4. Discussion

Detrick and Lanzerotti [2001] looked at the time series data from the AGO5/AGO6 pair to study geomagnetic quiet-time (Sq) variations at very high geomagnetic latitudes in effort to compare with and improve upon contemporaneous Sq models. To make data/model comparisons, the authors selected the five quietest days in each month (as identified by the Kp index) between February 1997 - January 1998; for each of the five quiet days in a given month, the authors low-pass filtered, downsampled, and fast Fourier transformed the data, isolated the 3-, 6-, 12-, and 24-hour Fourier spectra, and constructed five representative quiet-time curves for the month via the inverse Fourier-transform; the average of these curves was then used as the data-derived quiet-time curves to be used in comparison with the model. AGO5 and AGO6 data-derived quiet-time curves exhibited significant difference, but appeared to both suggest that Sq variations near the corrected geomagnetic pole (as inferred from these two high-latitude sites) was a factor of two or more than suggested by the models, independent of season. *Detrick and Lanzerotti* [2001] interpreted differences in the vertical components at the two sites as indicative of large differences in the deep mantle conductivity under the ice at AGO5 and AGO6.

Yagova et al. [2004] looked at a one-month average of spectral and cross-spectral features between AGO5 and AGO6. In agreement with our analysis, they note that the average power at AGO6 takes on a MLT dependence characteristic of sites at ∼80°S CGMLat. They show quite a few other features that are inexplicable by CGM coordinates, such as a dramatic asymmetry in the statistical distributions for sites along ∼80° CGMLat (which can also be seen in the work of *Ballatore et al.* [1998], though it is not commented on there). They interpret such differences in the statistical power as due to the importance of geographic, in addition to geomagnetic, coordinates in organizing hydromagnetic phenomena at polar cap latitudes. We agree that geographic coordinates are important and that CGM coordinates alone cannot explain the hydromagnetic activity in the nominal polar cap. The work of *Yagova et al.* [2004] further shows that the hydromagnetic power at Vostok (VOS) (∼83°S CGMLat), is akin to AGO5—another hydromagnetic feature inexplicable in reference to CGM coordinates which place VOS at a lower CGMLat than AGO6.

We have examined significant differences in both the vertical horizontal power at AGO5 and AGO6 both synoptically and statistically. We conclude that the differences are largely driven by differences in the ionospheric/magnetospheric region under observation and that CGM coordinates mischaracterize the high-latitude region. CGM coordinates prescribe both AGO5 and AGO6 as existing deep in the polar cap near the central point, while the coordinates locate MCM much further from center. However our data shows that AGO5 and AGO6 do not compare favorably, but that AGO6 and MCM do, and that AGO5 stands out as unique. For example, in Figure 7, we show that the median power in the Pc4-6 bands across all components is

always 2-3x lower at AGO5 than found at MCM or AGO6 (more so in the vertical component). The mean power (not shown) is always 2-5x lower at AGO5 than MCM or AGO6 (again, more so in the vertical). However, AGO6 and MCM are always comparable, independent of which component or band one is investigating. Such unanticipated and seemingly inexplicable differences arise only if one assumes the CGM pole can be meaningfully used to organize polar cap phenomena. Our data shows that—at least during austral summer—this is not the case, suggesting that the CGM pole is poorly suited as a central point in the polar cap.

Other authors have also highlighted the inadequacy of CGM coordinates at polar latitudes as well as the apparent importance of geographic coordinates. *Lepidi et al.* [2003] compared initial results from the magnetometer at Dome C (DMC) situated at 88.8°S CGMLat and compared them to data from the cusp-latitude magnetometer at Terra Nova Bay (TNB) (now referred to as "Mario Zuchelli Station") located at ∼80°S CGMLat. Despite the significant difference in CGMLat, geographically speaking, TNB and DMC are located at approximately the same latitude. This allowed the authors to parse geographically- and geomagnetically-oriented effects. *Lepidi et al.* [2003] found that diurnal variation at the two sites is similar and the ∼1-mHz fluctuations are coherent between the two stations, provided that in one compares the data in geographically-oriented components. The authors argued that this implicated that geographically-oriented ionospheric currents are responsible for the low (Pc6 band) frequency fluctuations rather than field-aligned currents. Furthermore, *Lepidi et al.* [2003] showed that in the polar cap region one cannot simply compare the magnetic north data from one site to the magnetic north data from another site. in fact, by comparing non-homologous components, *Lepidi et al.* [2003] found the amplitude of the daily variation at DMC and TNB to be comparable. This implies that one should always look at both horizontal components at polar cap latitudes (e.g., Figure 7), and for brevity is why we visualized the total horizontal power throughout (Figure 2 and Figure 5).

One easily draws from any of our data visualizations in this paper that the coupled or decoupled nature of Pc5-6/Pi3 variations depends on which cap- and cusp-latitude sites one chooses to compare (e.g., a study comparing AGO5 and MCM versus a study comparing AGO6 and MCM). *Lepidi et al.* [2003] indicate this themselves, noting the importance of the geographic coordinates at the two sites. This tells us that studies such as *Lepidi et al.* [2003] (and related ones, such as *Francia et al.* [2005], *De Lauretis et al.* [2005], *Pietrolungo et al.* [2008], *Francia et al.* [2009], *Pietrolungo et al.* [2013], and our own) have results that will not necessarily agree with each other if one is to assume that statistics at one cap/cusp site are applicable to another cap/cusp site.

This caveat applies to any given magnetometer or localized network of magnetometers in the nominal polar cap region. For example, the results from a Antarctic meridional chain of magnetometers in *Yagova et al.* [2002] likely do not speak for the chain separated 12 hours in local time. *Yagova et al.* [2010] use nearly two years of magnetometer data from 29 observatories in the northern hemisphere ranging over both polar and auroral latitudes to construct statistical maps of Pc5-6/Pi3 hydromagnetic activity in the (MLat, MLT) coordinate system. Specifically, in the polar cap the map is constructed using 5 sites between 81-87° CGMLat and -40.3-105.7° CGMLon, covering just under a 10-hour sector of MLT. However, the striking statistical and daily differences in magnetometer data derived from AGO5 and AGO6 (both at ∼86°S CGMLat, separated in MLT by 12 hours), tells us that the CGM coordinate system cannot be used in a meaningful way to statistically characterize one CGMLat as a function of MLT by using a single magnetometer at that CGMLat. Results derived from one site (say AGO6) do not necessarily describe the hydromagnetic activity at other sites with the same CGMLat, but differing MLon (in this case, AGO5). In light of this, the network used in *Yagova et al.* [2010] to characterize ULF activity leaves a 16-hour sector vulnerable to mild-to-severe bias. To be safe, such statistical maps in the CGM coordinate system should only be used to characterize the location nearby the magnetometer from which they were derived.

Interestingly, considering the various geomagnetic poles plotted in *Detrick and Lanzerotti* [2001] in context of the observations presented here from AGO5 and the observation Vostok Station (VOS) was shown by *Yagova et al.* [2004] to have similar statistical features as AGO5, it appears that the Schmidt eccentric dipole (ED) axial dipole (EDA) point (*Fraser-Smith* [1987]) might serve as an excellent centralizing point in the polar cap. In context of our data from AGO5, AGO6, and MCM, one might argue that AGO5 itself is a better central point in the polar cap than the CGM pole. In effect, we require a central point that positions VOS closer in latitude to AGO5 and higher in latitude than AGO6, while placing AGO6 and MCM at roughly the same latitude . In Table 3, we use solid-body rotations of geographic coordinates to get a rough idea whether or not the AGO5 location (or a more physically-motivated location like that of the EDA pole or the centered dipole (CD)), meets these requirements. As suspected visually, both AGO5 and the EDA pole serve a better centralizing point in the polar cap than the CGM pole. Both points cast AGO5 and VOS as deep in the polar cap, while MCM approximately retains its latitude, and AGO6 is assigned a similar latitude as MCM. The CD pole and ED dip (EDD) pole do not meet our requirements. A coordinate re-organization is something we are continuing to look into in more depth.

5. Conclusions

The importance of the AGO5/AGO6 comparisons in this study cannot be overstated: they reveal that the CGM coordinates do not organize the polar cap region in an ideal way and that the CGM pole should not be considered a central point to organize southern polar cap phenomena. It is likely the CGM pole in the northern hemisphere is equally unideal. However, due to the land mass distribution and the typical coverage in the northern hemisphere coverage, which is fairly localized (and therefore biased), there is little opportunity to explore and identify a truly central point in the northern polar cap as we've done for the southern polar cap using the AGO5/AGO6 pair. In light of this we urge caution when using single sites or meridional chains in the southern hemisphere for extrapolating (CGMLat, MLT) features, and double down on this caveat in the northern hemisphere.

AGO6 last collected data in 2001. Given the importance of AGO6 observations in this study, observation sites near and around the location of AGO6 should be installed in the polar cap, so that we can better understand the synoptic nature of the hydromagnetic polar cap. Without AGO6, to our knowledge, there is currently no near-pole latitude site in the same CGM longitude region (∼215°E CGMLon) in both the southern and northern hemispheres; see Table 2. In the south, DRV is nearby in CGM longitude (∼236.0°E CGMLon), but 5-6 degrees to low in CGM latitude (∼80°S CGMLat).

In summary, we have shown: (1) In the U.S. network of geophysical observatories in Antarctica, AGO5 stands out as a hydromagnetically-unique, high-latitude site within the nominal polar cap in the day-to-day ULF power spectra (Figure 2 and Figure 3), the MR spectra (Figure 5 and Figure 6), and the median power as a function of MLT (Figure 7). (2) However, the median ULF background spectrum observed at AGO5, AGO6, and MCM is approximately the

same (Figure 4). (3) The uniqueness of AGO5 is largely in its lack of diurnal variation in the ULF band, which can be seen in the power spectra , but is better visualized in the MR spectra: the daily evolution of the MR spectra at AGO6 and MCM show strong diurnal variation on top of long-term evolution, while only long-term evolution stands out at AGO5. (4) In general, our observations place AGO6 in the same geomagnetic region as MCM—a well-studied cusp-latitude site—contrary to its CGM position, which places AGO6 deep in the polar cap. (5) This suggests that CGM coordinates are inadequate in organizing high-latitude ULF phenomena. (6) In light of our observations, a better coordinate system for organizing polar cap phenomenon is one whose pole is located further away from AGO6, closer towards AGO5, and closer toward VOS. (7) We propose that the AGO5 location and the EDA pole both organize the observations better than the CGM pole. (7) The location of the AGO6 magnetometer is unique, and although it seems it is not deep in the polar cap as originally thought, the location is an under-sampled region in CGM coordinates.

Given these observations, CGM coordinates should be used with caution at polar and auroral latitudes.

Acknowledgments. This study was supported by the National Science Foundation with grants PLR-1247975 and PLR-1443507 to the New Jersey Institute of Technology and grant PLR-1248062 to Merrimack College. Access to AGO/SPA/MCM data can be obtained from [1]. Kp, Dst, and Ae index data comes from the World Data Center [2]. Simon Shepherd's corrected geomagnetic coordinates can be computed online at [3].

1. http://www.antarcticgeospace.org.
2. http://wdc.kugi.kyoto-u.ac.jp/wdc/Sec3.html
3. http://sdnet.thayer.dartmouth.edu/aacgm/aacgm_calc.php

References

Ables, S. T., B. J. Fraser, C. L. Waters, D. A. Neudegg, and R. J. Morris (1998), Monitoring cusp/cleft topology using pc5 ulf waves, *Geophysical Research Letters*, *25*(9).

Baker, K., and S. Wing (1989), A new magnetic coordinate system for conjugate studies at high latitudes, *Journal of Geophysical Research*, *94*(A7).

Ballatore, P., L. J. Lanzerotti, and C. G. Maclennan (1998), Multistation measurements of pc5 geomagnetic power amplitudes at high latitudes, *Journal of Geophysical Research: Space Physics (1978–2012)*, *103*(A12), 29,455–29,465.

Bolshakova, O. V., V. A. Troitskaia, and V. P. Hessler (1975), Analysis of the position of the polar boundary of the dayside cusp based on the intensity of high-latitude oscillations, *Geomagnetism and Aeronomy*, *15*, 755–757.

De Lauretis, M., P. Francia, M. Vellante, A. Piancatelli, U. Villante, and D. Di Memmo (2005), Ulf geomagnetic pulsations in the southern polar cap: Simultaneous measurements near the cusp and the geomagnetic pole, *Journal of Geophysical Research: Space Physics*, *110*(A11).

Detrick, D., and L. Lanzerotti (2001), Geomagnetic quiet time (sq) variations at high latitudes, *Geophysical research letters*, *28*(13), 2581–2584.

Doolittle, J., and S. Mende (1985), Development of an automatic geophysical observatory, *Antarctic Journal of the United States*, *20*(5), 229.

Dudeney, J. R., R. I. Kressman, and A. S. Rodger (1998), Automated observatories for geospace research in the polar regions, *Antarctic Science*, *10*(2), 192–203.

Engebretson, M., W. Hughes, J. Alford, E. Zesta, J. L.J. Cahill, R. Arnoldy, and G. Reeves (1995), Magnetometer array for cusp and cleft studies observations of the spatial extens of broadband ulf magnetic pulsations at cusp/cleft latitudes, *Journal of Geophysical Research*, *100*(A10).

Engebretson, M., J. Posch, V. Pilipenko, and O. Chugunova (2006), Ulf waves at very high latitudes, in *Magnetospheric ULF Waves: Synthesis and New Directions*, edited by K. Takahashi, P. Chi, R. Denton, and R. Lysak.

Francia, P., L. Lanzerotti, U. Villante, S. Lepidi, and D. Di Memmo (2005), A statistical analysis of low-frequency magnetic pulsations at cusp and cap latitudes in antarctica, *Journal of Geophysical Research: Space Physics*, *110*(A2).

Francia, P., M. De Lauretis, M. Vellante, U. Villante, and A. Piancatelli (2009), Ulf geomagnetic pulsations at different latitudes in antarctica, in *Annales geophysicae: atmospheres, hydrospheres and space sciences*, vol. 27, p. 3621.

Fraser-Smith, A. C. (1987), Centered and eccentric geomagnetic dipoles and their poles, 1600–1985, *Reviews of Geophysics*, *25*(1), 1–16.

Gustafsson, G. (1984), Corrected geomagnetic coordinates for epoch 1980, *Magnetospheric currents*, pp. 276–283.

Gustafsson, G., N. Papitashvili, and V. Papitashvili (1992), A revised corrected geomagnetic coordinate system for epochs 1985 and 1990, *Journal of atmospheric and terrestrial physics*, *54*(11), 1609–1631.

Harris, F. J. (1978), On the use of windows for harmonic analysis with the discrete fourier transform, *Proceedings of the IEEE*, *66*(1), 51–83.

Heinzel, G., A. Rüdiger, and R. Schilling (2002), Spectrum and spectral density estimation by the discrete fourier transform (dft), including a comprehensive list of window functions and some new at-top windows.

Heres, W., and N. A. Bonito (2007), An alternative method of computing altitude adjustment corrected geomagnetic coordinates as applied to igrf epoch 2005, *Tech. rep.*, DTIC Document.

Lanzerotti, L. J., A. Shono, H. Fukunishi, and C. G. Maclennan (1999), Long-period hydromagnetic waves at very high geomagnetic latitudes, *Journal of Geophysical Research*, *104*(A12).

Lepidi, S., L. Cafarella, P. Francia, A. Meloni, P. Palangio, and J. Schott (2003), Low frequency geomagnetic field variations at dome c (antarctica), in *Annales Geophysicae*, vol. 21, pp. 923–932.

Mathie, R., and I. Mann (2000), Observations of an anomalously low frequency alfven continuum in an abnormally expanded magnetosphere, *Geophysical research letters*, *27*(24), 4017–4020.

McHarg, M. G., J. V. Olson, and P. T. Newell (1995), Ulf cusp pulsations: Diurnal variations and interplanetary magnetic field correlations with ground-based observations, *Journal of Geophysical Research*, *100*(A10).

Melville, R., A. Stillinger, A. Gerrard, and A. Weatherwax (2014), Sustainable energy at the 100 w level for scientific sites on the antarctic plateau: Lessons learned from the polar experiment network for geospace upper atmosphere investigations-automatic geophysical observatory project, *Review of Scientific Instruments*, *85*(4), 045,117.

Mende, S., W. Rachelson, R. Sterling, H. Frey, S. Harris, S. McBride, T. Rosenberg, D. Detrick, J. Doolittle, M. Engebretson, et al. (2009), Observations of earth space by self-powered stations in antarctica, *Review of Scientific Instruments*, *80*(12), 124,501.

Newell, P., T. Sotirelis, K. Liou, C.-I. Meng, and F. Rich (2006), Cusp latitude and the optimal solar wind coupling function, *Journal of Geophysical Research: Space Physics (1978–2012)*, *111*(A9).

Papitashvili, V., N. Papitashvili, G. Gustafsson, K. Baker, A. Rodger, and L. Gromova (1992), A comparison between two corrected geomagnetic coordinate systems at high-latitudes., *Journal of geomagnetism and geoelectricity*, *44*(12), 1215–1224.

Papitashvili, V., C. Clauer, S. Musko, B. Belov, O. Troshichev, and M. Gudkov (1996), Low-magnitude, long-period magnetic pulsations observed deep in the southern polar cap, *Antarctic Journal of the United States*, *31*, 255–256.

Pietrolungo, M., S. Lepidi, L. Cafarella, L. Santarelli, and D. D. Mauro (2008), Daily variation at three antarctic geomagnetic observatories within the polar cap, in *Annales geophysicae: atmospheres, hydrospheres and space sciences*, vol. 26, p. 2179.

Pietrolungo, M., S. Lepidi, L. Cafarella, and D. Di Mauro (2013), A statistical analysis of low frequency geomagnetic field pulsations at two antarctic geomagnetic observatories in the polar cap region, *Advances in Space Research*, *52*(5), 853–864.

Pilipenko, V., and M. Engebretson (2002), Ground images at high latitudes of ulf wave processes in the outer magnetosphere, *Journal of atmospheric and solar-terrestrial physics*, *64*(2), 183–201.

Pilipenko, V., V. Belakhovsky, M. Engebretson, A. Kozlovsky, and T. Yeoman (2015), Are dayside long-period pulsations related to the cusp?, in *Annales Geophysicae*, vol. 33, pp. 395–404, Copernicus GmbH.

Shepherd, S. (2014), Altitude-adjusted corrected geomagnetic coordinates: Definition and functional approximations, *Journal of Geophysical Research*, *119*.

Troitskaya, V. (1985), Ulf wave investigations in the dayside cusp, *Advances in space research*, *5*(4), 219–228.

Troitskaya, V., and O. Bolshakova (1988), Diagnostics of the magnetosphere using multipoint measurements of ulf-waves, *Advances in Space Research*, *8*(9), 413–425.

Troitskaya, V. A., and O. V. Bolshakova (1977), Diurnal latitude variation of the location of the dayside cusp, *Planetary and Space Science*, *25*(12).

Troitskaya, V. A., O. V. Bolshakova, and E. T. Matveeva (1980), Geomagnetic pulsations in the polar cap., *Journal of geomagnetism and geoelectricity*, *32*(6), 309–324.

Urban, K., A. Gerrard, Y. Bhattacharya, A. Ridley, L. Lanzerotti, and A. Weatherwax (2011), Quiet-time observations of the open-closed boundary prior to the CIR-induced storm of 9 august 2008, *Space Weather*, *9*(11).

Weatherwax, A., T. Rosenberg, C. Maclennan, and J. Doolittle (1997), Substorm precipitation in the polar cap and associated pc 5 modulation, *Geophysical research letters*, *24*(5), 579–582.

Wolfe, A., L. Lanzerotti, C. Maclennan, and A. Weatherwax (1996), Large-amplitude hydromagnetic waves on open geomagnetic field lines, *Antarctic Journal of the United States*, *31*, 257–259.

Yagova, N., L. Lanzerotti, U. Villante, V. Pilipenko, S. Lepidi, P. Francia, V. Papitashvili, and A. Rodger (2002), Ulf pc5-6 magnetic activity in the polar cap as observed along a geomagnetic meridian in antarctica, *Journal of Geophysical Research: Space Physics*, *107*(A8).

Yagova, N., V. Pilipenko, L. Lanzerotti, M. Engebretson, A. Rodger, S. Lepidi, and V. Papitashvili (2004), Two-dimensional structure of long-period pulsations at polar latitudes in antarctica, *Journal of Geophysical Research: Space Physics*, *109*(A3).

Yagova, N., V. Pilipenko, L. Baransky, and M. Engebretson (2010), Spatial distribution of spectral parameters of high latitude geomagnetic disturbances in the pc5/pi3 frequency range, in *Annales geophysicae: atmospheres, hydrospheres and space sciences*, vol. 28, p. 1761.

K. Urban, Center for Solar-Terrestrial Research, New Jersey Institute of Technology, 323 Martin Luther King Boulevard, 101 Tiernan Hall, Newark, NJ 07102-1982, USA (kdu2@njit.edu)

A. J. Gerrard, Center for Solar-Terrestrial Research, New Jersey Institute of Technology, 323 Martin Luther King Boulevard, 101 Tiernan Hall, Newark, NJ 07102-1982, USA (andrew.j.gerrard@njit.edu)

L. J. Lanzerotti, Center for Solar-Terrestrial Research, New Jersey Institute of Technology, 323 Martin Luther King Jr. Boulevard, 101 Tiernan Hall, Newark, NJ 07102-1982, USA. (louis.j.lanzerotti@njit.edu)

A. T. Weatherwax, School of Science and Engineering, Merrimack College, 315 Turnpike St, North Andover, MA 01845. USA. (aweatherwax@siena.edu)

Table 1. The locations of the four U.S. Antarctic geophysical observatories (AGO5, AGO6, MCM, SPA) used in this study. During the 63-day interval under study, only these four of these sites had uninterrupted data coverage. This table provides the geographic latitude (GLat) and longitude (GLon), the JHU/APL AACGM latitude (MLat) and longitude (MLon) computed at 100-km for the 2000 epoch, Shepherd's field-line traced AACGM latitude (MLat*) and longitude (MLon*) computed at the same altitude and epoch, and the approximate UT of the site's magnetic local midnight (MLM). All latitudes and longitudes given in °S and °E, respectively.

Site	GLat	GLon	MLat	MLon	MLat*	MLon*	MLM
AGO5	77.24	123.52	86.85	28.90	86.70	29.68	3
AGO6	69.51	130.03	84.89	215.52	84.99	215.13	14.5
MCM	77.85	166.67	80.01	326.42	80.01	327.56	7
SPA	90.0	000.0	74.21	18.47	74.23	18.39	3.5

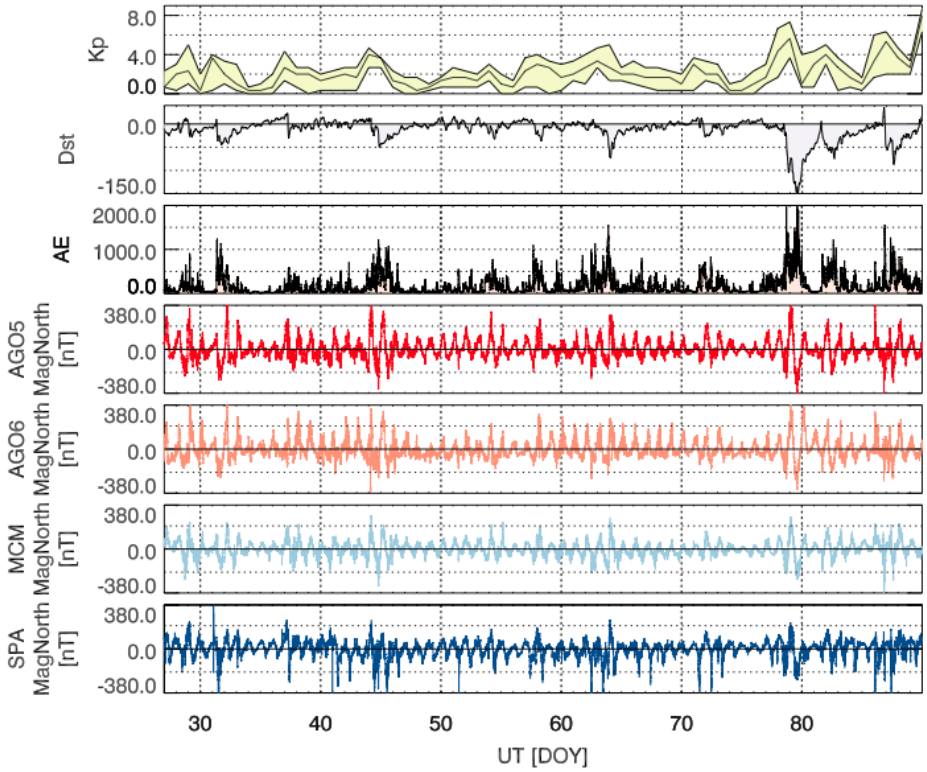

Figure 1. Raw, unfiltered magnetic north data from the four geomagnetic observatories used in this study in context of the concurrent geomagnetic conditions. The top three panels depict the global geomagnetic activity levels over the 63-day interval ranging over days 27-89 of year 2001. The top panel shows the minimum, median, and maximum Kp for each day. The second and third panels show the Dst and AE indices, respectively. The bottom four panels depict the local geomagnetic activity in the magnetic north component at sites AGO5 (red), AGO6 (light red), MCM (light blue), and SPA (blue) from highest to lowest CGM latitude (~87°S-74°S), top to bottom.

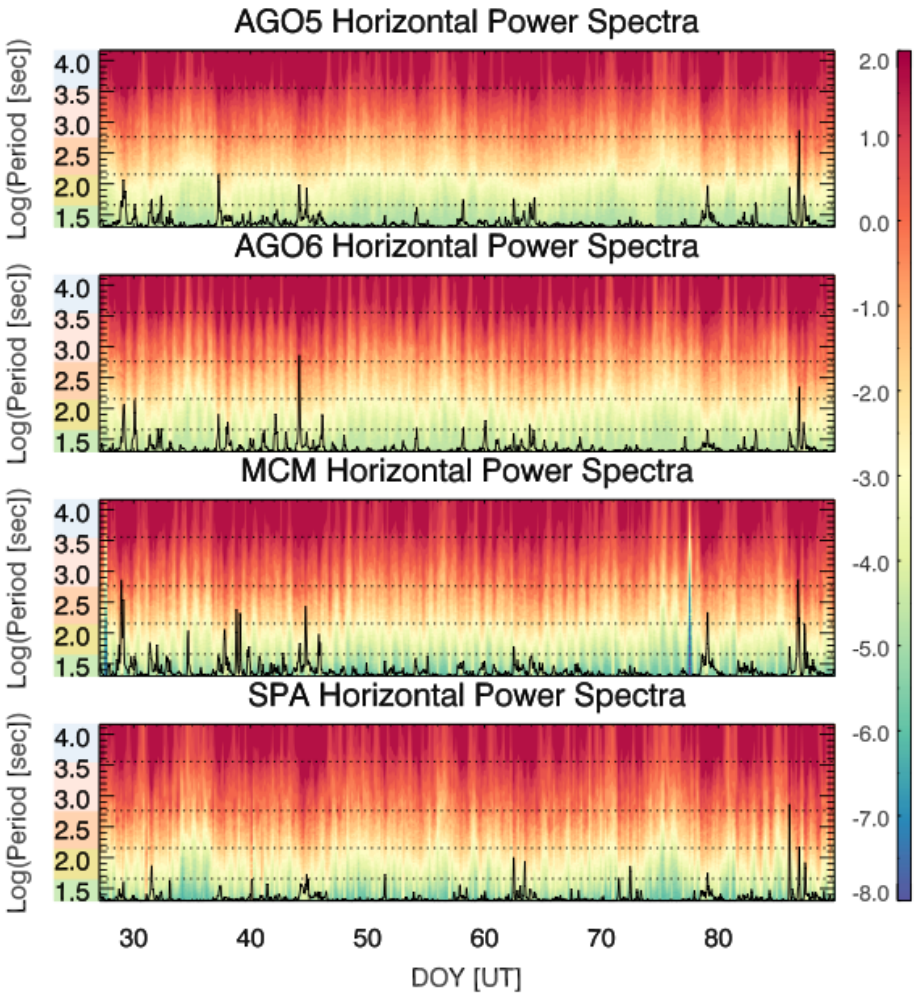

Figure 2. Horizontal power spectra, $LOG_{10}(\widehat{P}_H^w \ [nT^2])$, on the color axis versus $LOG_{10}(period \ [sec])$ on the vertical axis, plotted in 1-hour increments over the 63-day interval on the horizontal axis (ranging between 2001-Jan-27 to 2001-Mar-30) for the U.S. observation sites AGO5, AGO6, MCM, and SPA. The sites are placed from highest to lowest CGM latitude (∼87°-74°), top to bottom. For visual aid, on each contour the dashed lines represent the boundaries between the pulsation bands of interest (Pc3-RLF), which are also color-coded on the vertical axis from top to bottom: RLF (light blue), Pc6 (light red), Pc5 (orange), Pc4 (yellow), and Pc3 (green). The black overplotted trace on each contour plot is the integrated horizontal ULF power at the corresponding site (normalized at each site by the maximum value attained at the that site over the interval).

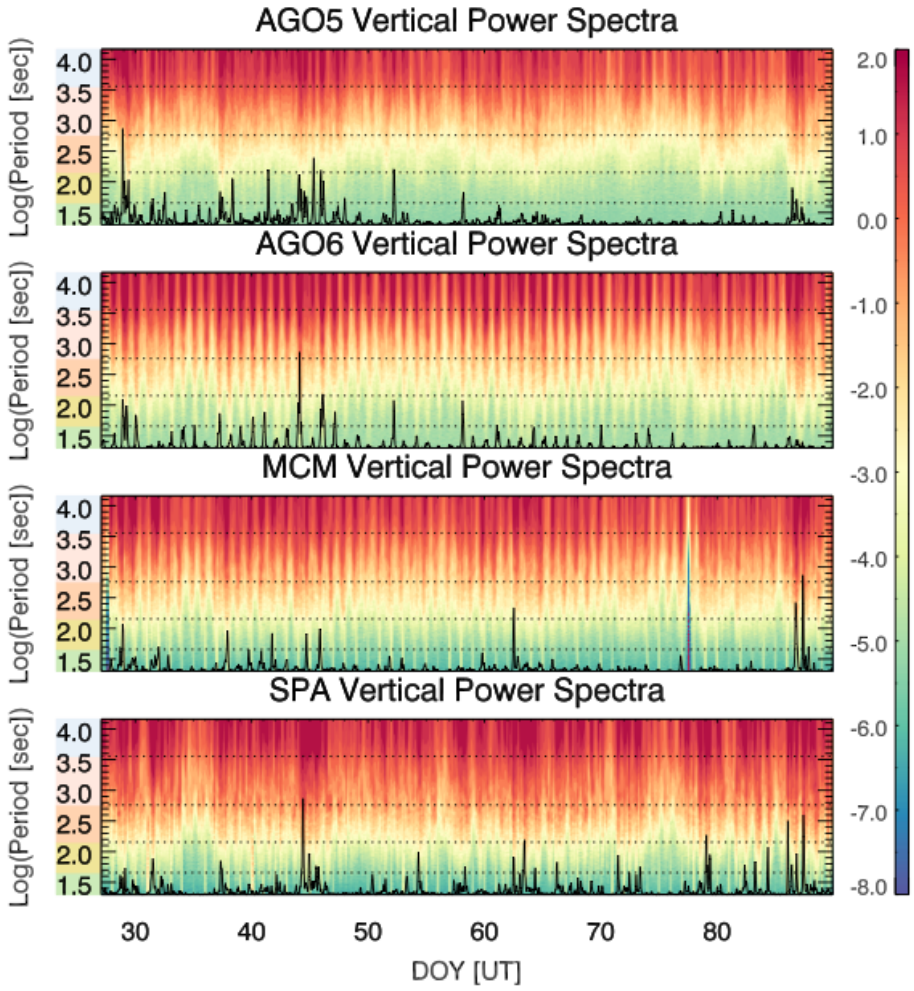

Figure 3. Vertical power spectra, $LOG_{10}(\widehat{P}_H^w \ [nT^2])$ (see Figure 3 for further description).

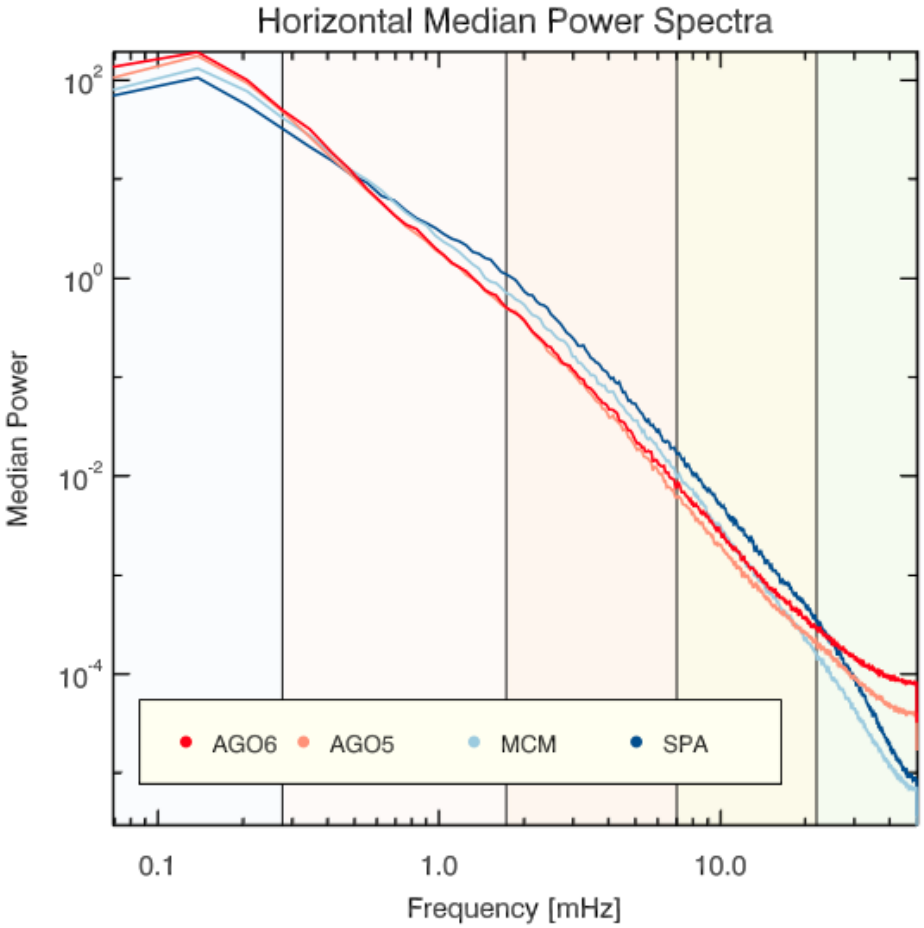

Figure 4. The horizontal median power spectra, $\widetilde{P}_H^{w,\tau}$, at AGO5 (red), AGO6 (light red), MCM (light blue), and SPA (blue) over the 63-day interval, τ, between 2001-Jan-27 to 2001-Mar-30. The color-coded columns represent the RLF (blue), Pc6 (light red), Pc5 (orange), Pc4 (yellow), Pc3 (green) frequency bands.

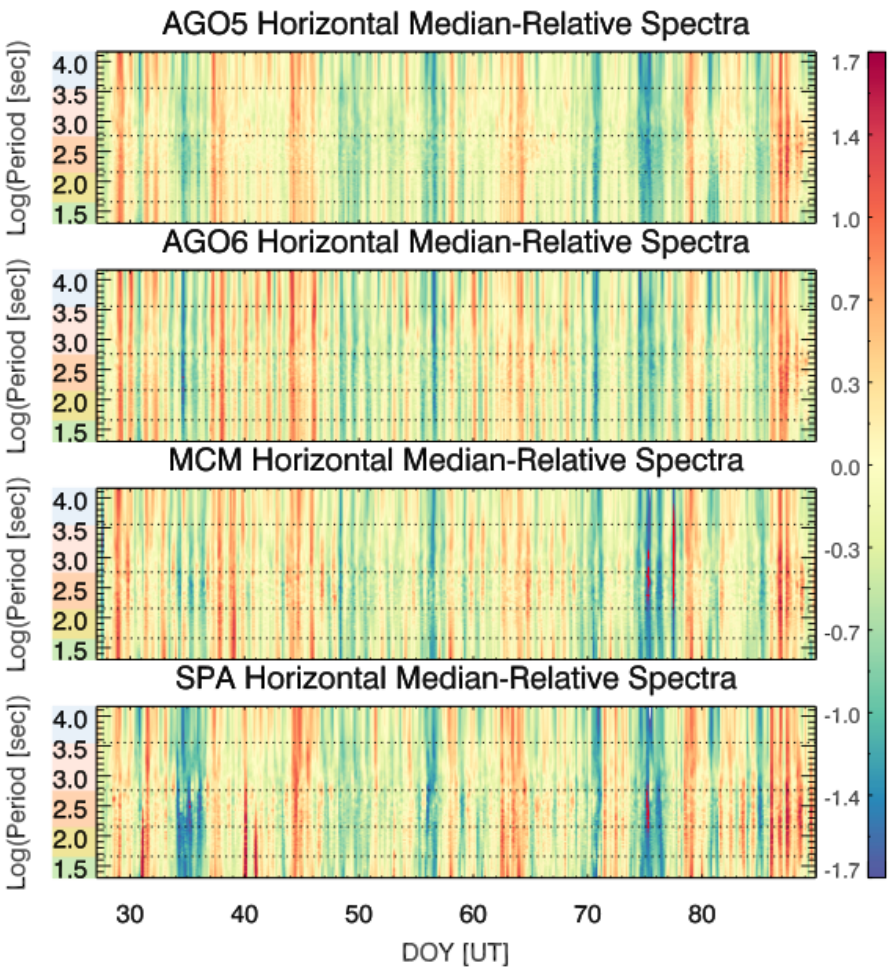

Figure 5. Horizontal median-relative power spectra, $LOG_{10}(\widehat{MR}_H^{w,\tau})$, on the color axis versus $LOG_{10}(period\ [sec])$ on the vertical axis, plotted in 1-hour increments over the 63-day interval, τ, on the horizontal axis (ranging between 2001-Jan-27 to 2001-Mar-30) for the U.S. observation sites AGO5, AGO6, MCM, and SPA. The sites are ordered top to bottom from highest to lowest CGM latitude (∼87°-74°). For visual aid, the dashed lines on each contour plot represent the boundaries between the pulsation bands of interest, which are also color-coded on the vertical axis from top to bottom: RLF (light blue), Pc6 (light red), Pc5 (orange), Pc4 (yellow), and Pc3 (green).

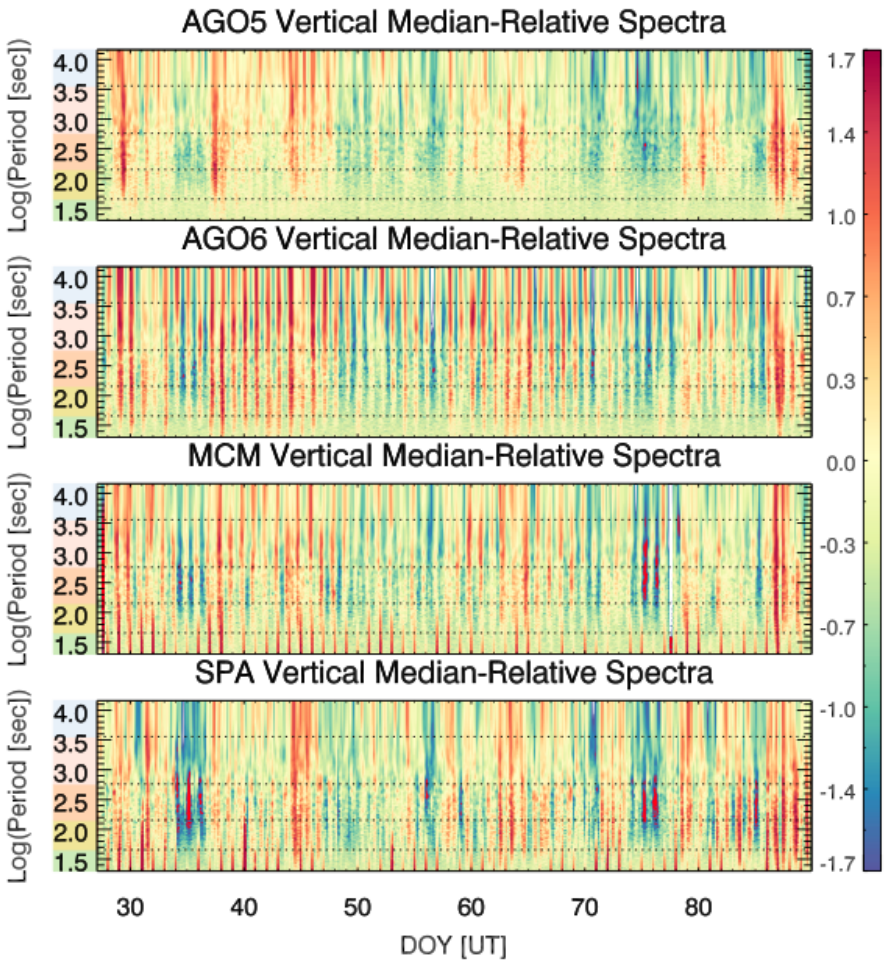

Figure 6. Vertical median-relative power spectra, $LOG_{10}(\widehat{MR}_V^{w,\tau})$ (see Figure 5 for further description).

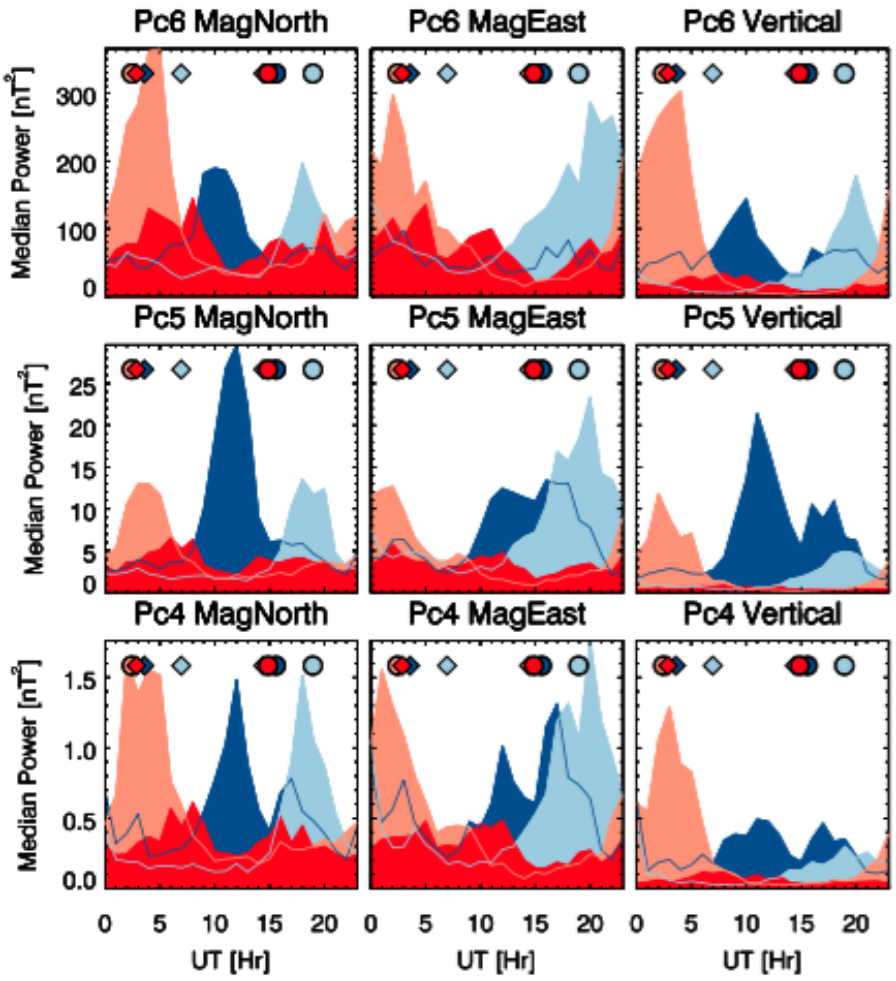

Figure 7. The local-time median distribution of ULF power in the Pc4, Pc5, and Pc6 bands for the magnetic north, magnetic east, and vertical components at each site in this study: SPA (blue), MCM (light blue), AGO6 (light red), AGO5 (red).

Table 2. High CGM-latitude [MLat*] sites in the northern and southern hemispheres, sorted by CGM longitude [MLon*] ($0 < lon < 360$). The CGM longitudinal region of AGO6 is unique compared to sites in both the northern and southern hemisphere, as indicated by ΔMLon*. CGM coordinates computed for year 2000 at 100-km altitude using Shepherd's field line tracing algoritm.

Site	MLat*	MLon*	ΔMLon*
AGO1	-80.21	16.90	198.23
AGO5	-86.70	29.68	185.45
THL	85.24	31.73	183.4
SVS	83.48	35.50	179.63
AGO4	-80.10	41.49	173.64
VOS	-83.51	54.48	160.64
DMC	-88.68	55.56	159.57
ALE	87.06	97.57	117.56
NRD	81.05	104.18	110.95
SUD	-81.13	108.03	107.1
CSY	-80.85	156.45	58.68
AGO6	-84.99	215.13	0.0
DRV	-80.64	235.76	-20.63
TNB	-80.09	307.89	-92.76
RES	83.34	319.90	-104.77
MCM	-80.01	327.56	-112.43
SBA	-79.99	327.56	-112.43

Table 3. Simple reorganization of latitude coordinates in the Antarctic polar cap for the AGO sites, MCM, SPA, Dome C (DMC), Vostok (VOS), Casey (CSY), Scott Base (SBA), Terra Nova Bay (TNB), d'Urville (DRV), and Mirney (MIR). Latitudes are computed as 90° minus the angular displacement from the given central polar cap point and result from physical rotations of geographic coordinates (i.e., these coordinates are not re-mapped via a CGM-like procedure). The latitudes are computed relative to AGO5, the centered dipole polar point (CD) (equated to the location of Vostok (VOS) here), the polar point of the (Scmidt) eccentric dipole (ED) axial pole (EDA), and the polar point of the ED dipole dip pole (EDD).

Site	CGMLat	AGO5	CD/VOS	EDA	EDD
AGO2	70.11	72.90	74.46	71.12	61.75
AGO3	72.05	74.80	77.70	73.67	63.93
SPA	74.23	77.24	78.45	75.34	66.06
SBA	79.99	80.85	78.22	78.91	73.76
MCM	80.01	80.88	78.10	78.93	73.89
TNB	80.09	80.05	76.80	78.52	75.50
AGO4	80.10	83.33	86.06	81.08	72.42
AGO1	80.21	83.11	83.67	81.29	72.20
DRV	80.62	78.42	75.05	79.05	85.17
CSY	80.85	78.41	77.79	80.58	82.95
AGO6	84.99	82.06	79.17	83.26	86.47
AGO5	86.70	90.00	86.29	87.78	78.78
DMC	88.68	88.09	85.00	88.60	80.68
VOS	83.51	86.29	90.00	85.91	76.22
MIR	77.38	70.07	77.47	78.05	76.10